

Simultaneous valence shift of Pr and Tb ions in (Pr_{1-y}Tb_y)_{0.7}Ca_{0.3}CoO₃ around M-I transition

H. Fujishiro,¹ T. Naito,¹ D. Takeda,¹ N. Yoshida,¹ T.
Watanabe,¹ K. Nitta,² J. Hejtmánek,³ K. Knížek,³ and Z. Jirák³

¹*Faculty of Engineering, Iwate University,
4-3-5 Ueda, Morioka 020-8551, Japan*

²*Japan Synchrotron Radiation Research Institute, Sayo, Hyogo 679-5198, Japan*

³*Institute of Physics, ASCR, Cukrovarnická 10, 162 00 Prague 6, Czech Republic*

(Dated: December 21, 2012)

Abstract

Temperature dependence of the X-ray absorption near-edge structure (XANES) spectra at the Pr L_3 - and Tb L_3 -edges was measured for the (Pr_{1-y}Tb_y)_{0.7}Ca_{0.3}CoO₃ system, in which a metal-insulator (MI) and spin-state (SS) transition took place simultaneously at a critical temperature T_{MI} . A small increase in the valence of the terbium ion was found below T_{MI} , besides the enhancement of the praseodymium valence; the trivalent states, which are stable at room temperature, change to a 3+/4+ ionic mixture at low temperatures. In particular for the $y=0.2$ sample, the average valence determined at 8 K amounts to 3.03+ and 3.25+ for the Tb and Pr ion, respectively. In analogous (Pr_{1-y}RE_y)_{0.7}Ca_{0.3}CoO₃ samples (RE=Sm and Eu), in which the MI-SS transition also took place, no valence shift of the RE ion was detected in the XANES spectra at the RE ion L_3 -edge. The role of the substituted RE ion for the Pr-site on the MI-SS transition is discussed.

PACS numbers: 71.30.+h, 78.70.Dm, 75.30.Wx

I. INTRODUCTION

The perovskite cobaltites RECoO_3 (RE=rare-earth element and Y) show a spin-state (SS) transition of Co^{3+} ions from a low spin state (LS; $t_{2g}^6 e_g^0$) to a high spin state (HS; $t_{2g}^4 e_g^2$) with increasing temperature, followed by the formation of the metallic state of the intermediate spin state (IS; $t_{2g}^5 \sigma^*$) at higher temperatures.¹ The temperature induced spin-state transition indicates a small energy difference δE between the crystal-field splitting and Hundfs coupling energy.^{2,3} The hole-doped systems with a mixed $\text{Co}^{3+}/\text{Co}^{4+}$ valence generally show a stable ferromagnetic metallic state. Most interestingly, a first-order metal-insulator (MI) transition was firstly observed on cooling in $\text{Pr}_{0.5}\text{Ca}_{0.5}\text{CoO}_3$ at $T_{\text{MI}}=90$ K under ambient pressure,^{4,5} in which the change in the electronic structure was confirmed at T_{MI} by the photoemission spectroscopy.⁶ The mechanism of the transition was tentatively ascribed to a spin-state crossover from itinerant cobalt states IS Co^{3+} to an ordered mixture of localized LS Co^{3+} and LS Co^{4+} ($t_{2g}^5 e_g^0$, $S=1/2$) states. Thereafter, the existence of $\text{Co}^{3+}/\text{Co}^{4+}$ ordering was questioned because the transition was evidenced in the less doped $\text{Pr}_{1-x}\text{Ca}_x\text{CoO}_3$ ($x=0.3$) under high pressures,⁷ or in the $(\text{Pr}_{1-y}\text{RE}_y)_{1-x}\text{Ca}_x\text{CoO}_3$ system ($0.2 \leq x \leq 0.5$) with a partial substitution of Pr by smaller RE cations such as Sm, Eu and Y under ambient pressure.⁷⁻⁹ This MI transition accompanied by SS transition appeared to be conditioned not only by the presence of both Pr and Ca ions, but also by a larger than critical structural distortion of the CoO_6 network, depending on the average ionic radius and size mismatch of perovskite A-site ions.⁹ Furthermore, the critical temperature T_{MI} was found to be depressed by the applied magnetic field.^{10,11}

An alternative scenario explaining the transition to the insulating state was proposed on the basis of electronic structure calculations exploiting the temperature dependence of the structural experimental data for $\text{Pr}_{0.5}\text{Ca}_{0.5}\text{CoO}_3$.¹² It appeared that the formal cobalt valence should change below T_{MI} from mixed-valence $\text{Co}^{3.5+}$ towards pure Co^{3+} with strong preference for the LS state and, concomitantly, the praseodymium valence should increase simultaneously from Pr^{3+} towards Pr^{4+} . The SS transition and the formation of an insulating state was thus interpreted as an analogy of the compositional transition from the ferromagnetic metal $\text{La}_{0.5}\text{Ca}_{0.5}\text{CoO}_3$ to the diamagnetic insulator of LaCoO_3 .^{13,14} Shortly afterwards, this theoretical hypothesis about the crucial role of the praseodymium valence shift in the MI transition, realized in fact as a mixture of the Pr^{3+} and Pr^{4+} states, was

experimentally confirmed by observation of a Schottky peak in the low-temperature specific heat of $(\text{Pr}_{1-y}\text{Y}_y)_{0.7}\text{Ca}_{0.3}\text{CoO}_3$ ($y=0.075$ and 0.15),¹⁵ which resulted from a significant population of Kramers Pr^{4+} ions.

Most recently, we directly confirmed the praseodymium valence shift from the X-ray absorption near-edge structure (XANES) spectra at the Pr L_3 -edge for the same $(\text{Pr}_{1-y}\text{Y}_y)_{0.7}\text{Ca}_{0.3}\text{CoO}_3$ samples.¹⁶ It has been found that the average valence of the praseodymium ion increases below room temperature from the common value 3.0+, undergoes a steepest change at T_{MI} and reaches finally 3.15+ and 3.27+ at 8 K for the $y=0.075$ and 0.15 samples, respectively. Interestingly, these values are consistent with those estimated by quantitative analysis of the entropy associated with the Schottky peak dominating the low-temperature specific heat. For $\text{Pr}_{0.5}\text{Ca}_{0.5}\text{CoO}_3$, similar valence shifts from 3.0+ at 300 K to 3.15+ at 10 K were obtained by other authors using XANES at Pr L_3 and $M_{4,5}$ edges.¹⁷ In addition, a change of cobalt spin states has been evidenced by the analysis of two complementary synchrotron X-ray spectroscopic techniques.¹⁸

In the present work, we apply XANES spectroscopy measurements to the analysis of $(\text{Pr}_{1-y}\text{RE}_y)_{0.7}\text{Ca}_{0.3}\text{CoO}_3$ systems (RE=Tb, Sm and Eu), in which the MI-SS transition between 50-140 K was obtained.^{8,9} The choice of substituting RE ions was motivated by the fact that terbium ion is known to adopt the mixed valence state $\text{Tb}^{3+}/\text{Tb}^{4+}$ in several compounds.¹⁹ The Sm and Eu ions are known to exist also in various valence states. As an example, in the Sm-based filled skutterudite, $\text{SmOs}_4\text{Sb}_{12}$, Sm ions possess a mixed valence state between Sm^{2+} and Sm^{3+} , which can be detected by XANES.²⁰ In the Eu-contained niobates such as $\text{Eu}_2\text{Nb}_5\text{O}_9$ and EuNbO_3 , a mixed valence state between Eu^{2+} and Eu^{3+} was detected by photoelectron spectroscopy.²¹ In this study, we thus present a detailed temperature dependence of the XANES spectra around the RE L_3 -edges measured using the bulk sensitive transmission method, and derive the RE ion states from the spectra.

II. EXPERIMENTAL

Polycrystalline samples $(\text{Pr}_{1-y}\text{Tb}_y)_{0.7}\text{Ca}_{0.3}\text{CoO}_3$ ($y=0, 0.1, 0.2$), $(\text{Pr}_{0.7}\text{Sm}_{0.3})_{0.7}\text{Ca}_{0.3}\text{CoO}_3$, and $(\text{Pr}_{0.85}\text{Eu}_{0.15})_{0.7}\text{Ca}_{0.3}\text{CoO}_3$ were fabricated by a solid-state reaction. Raw powders of Pr_6O_{11} , Tb_4O_7 , Sm_2O_3 , Eu_2O_3 , Co_3O_4 , and CaCO_3 were weighted with proper molar ratios and ground using an agate mortar and pestle for 1

h. Mixed powders were calcined at 1000 °C for 24 h in air. Then they were pulverized, ground, and pressed into pellets of 20 mm diameter and 4 mm thickness. Pellets were sintered at 1200 °C for 24 h in 0.1 MPa flowing oxygen gas. The measured relative densities of each sample were greater than 90%. Powder X-ray diffraction patterns were taken for each sample using Cu $K\alpha$ radiation; the samples were confirmed to have a single-phase orthoperovskite $Pbnm$ structure. For the XANES measurements, a small amount of the samples were pulverized, mixed with boron nitride powder (99.9%) with proper molar ratios in order to optimize absorption, and pelletized 6 mm in diameter and 0.5 mm in thickness.

Each XANES spectrum of the samples was measured at BL01B1 of SPring-8 in Japan. The beam was monochromatized using a Si(111) double-crystal monochromator. The spectra were recorded in the transmission mode with the detectors of the ionization chambers and obtained at various temperatures from 8 to 300 K using a cryocooler. The measurements were performed upon the heating run. The energy resolution was within 1.5 eV around $E=8$ keV.

To determine the mixed $\text{Pr}^{3+}/\text{Pr}^{4+}$ contents at low temperatures for $(\text{Pr}_{1-y}\text{Tb}_y)_{0.7}\text{Ca}_{0.3}\text{CoO}_3$, the calibration line was obtained using XANES spectra of Pr_6O_{11} as $\text{Pr}^{3.667+}$ and $(\text{Pr}_{1-y}\text{Tb}_y)_{0.7}\text{Ca}_{0.3}\text{CoO}_3$ as $\text{Pr}^{3.0+}$ measured at 300 K, which were performed similarly to the previous paper.¹⁶ The recorded XANES spectra were modeled by the sum of three Lorentzian functions and one arctangent function representing the step like edge of continuum excitations. One Lorentzian function (peak A: 5966 eV) shows an excitation from $2p_{3/2}$ to $4f^25d^*$, which represents $\text{Pr}^{3.0+}$ ions. The other Lorentzian functions (peak B2: 5969 eV and peak B1: 5979 eV) show the excitations from $2p_{3/2}$ to $4f^2\text{L}5d^*$ and to $4f^15d^*$, L being a ligand hole in the O $2p$ orbital, both of which represent Pr^{4+} ions.^{22,23} The energy differences between peaks A, B2, and B1 were fixed according to results of Hu *et al.*²⁴ The curve fittings were performed in the energy range from 5944 to 5985 eV using Athena software.²⁵

To estimate the mixed $\text{Tb}^{3+}/\text{Tb}^{4+}$ contents, a similar procedure was applied. A comparative measurement of Tb_4O_7 and $(\text{Pr}_{1-y}\text{Tb}_y)_{0.7}\text{Ca}_{0.3}\text{CoO}_3$ was carried out at 300K as standards of $\text{Tb}^{3.5+}$ and $\text{Tb}^{3.0+}$, respectively. The recorded XANES spectra for Tb L_3 line were modeled by the sum of two Lorentzian functions (peak C: 7518 eV for Tb^{3+} ($4f^8$) and peak D: 7528 eV for Tb^{4+} ($4f^7$)) and one arctangent function. For simplicity, the peak related to the ligand hole state $4f^8\text{L}$ was omitted because of its weaker intensity as reported

by Dexpert *et al.*²⁶ For $(\text{Pr}_{0.7}\text{Sm}_{0.3})_{0.7}\text{Ca}_{0.3}\text{CoO}_3$, and $(\text{Pr}_{0.85}\text{Eu}_{0.15})_{0.7}\text{Ca}_{0.3}\text{CoO}_3$ samples, the XANES spectra were measured around Pr L_3 (5966 eV), Sm L_3 (6720 eV) and Eu L_3 (6981 eV) edges, respectively.

III. RESULTS AND DISCUSSION

A. Electrical and magnetic properties in $(\text{Pr}_{1-y}\text{Tb}_y)_{0.7}\text{Ca}_{0.3}\text{CoO}_3$

The electrical resistivity $\rho(T)$ and susceptibility $\chi(T)$ of the $(\text{Pr}_{1-y}\text{Tb}_y)_{0.7}\text{Ca}_{0.3}\text{CoO}_3$ ($y=0, 0.1, 0.2$) samples are presented in Figs. 1(a) and 1(b). For the $y=0$ sample with absence of MI transition, $\rho(T)$ exhibits a globally metallic behavior over the entire temperature range with the long range ferromagnetism established below 50 K. For the Tb-substituted samples, the resistivity exhibits a sharp jump on the cooling below the transition temperatures of $T_{\text{MI}}=70$ and 140 K for $y=0.1$ and 0.2, respectively, and increases further down to low temperatures. On the heating run, $\rho(T)$ shows a sharp drop at $T_{\text{MI}}=75$ and 148 K, respectively, but the resistivity value above T_{MI} is not restored and is systematically larger than that on the cooling run. Such irreversibility may result from the micro cracks in the samples due to the large volume contraction when passing through the transition temperature.⁹ The transitions in the $(\text{Pr}_{1-y}\text{Tb}_y)_{0.7}\text{Ca}_{0.3}\text{CoO}_3$ system are further evidenced in the plot of magnetic susceptibility. For the Tb free sample $y=0$, $\chi(T)$ steeply increases to large values at low temperatures in accordance with the ferromagnetic ground state of this compound ($T_{\text{C}}=55$ K). The Tb substituted samples exhibit a marked drop of magnetic susceptibility at nearly the same temperature as $\rho(T)$ on the cooling run, which is a strong sign that cobalt ions transform to LS states below T_{MI} .¹⁵ These characteristics of the Tb-substituted samples are the same as those observed for $(\text{Pr}_{1-y}\text{Y}_y)_{0.7}\text{Ca}_{0.3}\text{CoO}_3$ and other $(\text{Pr}_{1-y}\text{RE}_y)_{0.7}\text{Ca}_{0.3}\text{CoO}_3$ systems.^{8,9} It is worth mentioning that, in distinction to Y and Sm substituted samples, the low-temperature susceptibility increases with y , which should be related to large moment of Tb ion independently on its trivalent or tetravalent state. (Tb^{3+} with $4f^8$ configuration is a specific case of non-Kramers ion. Although its eigenstates are nonmagnetic in the low-symmetry crystal field of $Pbnm$ perovskite structure, the ground and first excited singlets are nearly degenerate, forming a magnetic quasi-doublet.²⁷)

B. XANES measurements of Pr L_3 - and Tb L_3 -edges

Figure 2(a) shows the temperature dependence of the XANES spectra at the Pr L_3 -edge for the $(\text{Pr}_{0.8}\text{Tb}_{0.2})_{0.7}\text{Ca}_{0.3}\text{CoO}_3$ sample. Two main peaks situated at 5966 and 5979 eV (named peaks A and B1) originate from the Pr $2p \rightarrow 5d$ transitions. At 300 K, the Pr^{3+} ($4f^2$) sites essentially contribute to the peak A, with a little component at peak B2, which is caused presumably by multiple scattering, commonly treated in the theoretical simulations of XANES.¹⁶ At temperatures below $T_{\text{MI}}=148$ K, the shape of the XANES spectra changes markedly; the intensity of peak B1 increases notably and shifts to lower energy side, while the intensity of peak A decreases. At the same time, a new component (peak B2 at 5969 eV) can be resolved on its high-energy slope. Since the B1 and B2 peaks are manifestations of Pr^{4+} states, originating in particular of the configurations $4f^1$ and $4f^2\bar{L}$,²²⁻²⁴ the observed changes confirm that the average valence of the Pr ions in the $(\text{Pr}_{1-y}\text{Tb}_y)_{0.7}\text{Ca}_{0.3}\text{CoO}_3$ increases from 3+ toward 4+ below T_{MI} , consistently with those reported for $(\text{Pr}_{1-y}\text{Yb}_y)_{0.7}\text{Ca}_{0.3}\text{CoO}_3$ by us¹⁶ or for $\text{Pr}_{0.5}\text{Ca}_{0.5}\text{CoO}_3$ by García-Muñoz *et al.*¹⁷

Figure 2(b) shows the temperature dependence of the XANES spectra at the Tb L_3 -edge for the same $(\text{Pr}_{0.8}\text{Tb}_{0.2})_{0.7}\text{Ca}_{0.3}\text{CoO}_3$ sample. Two main peaks situated at 7518 and 7529 eV (named peaks C and D) originate from the Tb $2p \rightarrow 5d$ transitions. At 300 K, the Tb^{3+} ($4f^8$) sites contribute to the main peak C. The character of XANES spectra below $T_{\text{MI}}=148$ K is changed. The peak D increases slightly and shifts to lower energy. At the same time, a small drop of the intensity of peak C is observed. The peak D is a manifestation of Tb^{4+} states, namely, of the configuration $4f^7$.^{26,28} The observed behavior suggests that the valence of the Tb ions increases below T_{MI} , simultaneously with the valence shift of Pr ions.

C. Valence shifts of the Pr and Tb ions

In order to determine the valence shift of Pr ion quantitatively, the XANES spectra were fitted to a sum of three Lorentzian functions (peak A for Pr^{3+} and peaks B1 and B2 for Pr^{4+}) and one arctangent function, as indicated in ref. 16. Then the valence of Pr ions in the Tb substituted samples was deduced from the intensity ratio I_{B1}/I_A of the B1 spectral peak to the A spectral peak using the calibration line that took into account the actual I_{B1}/I_A values for Pr^{3+} and that for $\text{Pr}^{3.667+}$ (not shown). Figure 3(a) shows the temperature dependence of

the XANES spectra at the Pr L_3 -edge for pure $\text{Pr}_{0.7}\text{Ca}_{0.3}\text{CoO}_3$ with ferromagnetic metallic ground state (see Fig. 1). Apart of the main peak A, there is again a small bump at around 5980 eV, originating in the multiple scattering as mentioned above. The same feature has been observed for another metallic compound $\text{Pr}_{0.55}\text{Ca}_{0.45}\text{CoO}_3$,¹⁷ and seems thus to be a general manifestation of trivalent praseodymium in the mixed $\text{Co}^{3+}/\text{Co}^{4+}$ systems. Importantly, no spectral change of the Pr L_3 -edge is observed down to 8 K, which suggests that the Pr^{3+} valence in $\text{Pr}_{0.7}\text{Ca}_{0.3}\text{CoO}_3$ remains temperature independent.

Figure 3(b) shows the XANES spectrum for Tb_4O_7 at 300 K, which was fitted to a sum of two Lorentzian functions (peak C for Tb^{3+} and peak D for Tb^{4+}) and one arctangent function. The measurement was also performed down to low temperatures and since no relevant spectroscopic changes were detected, the spectrum, in particular the intensity ratio I_D/I_C , was further considered as a standard for $\text{Tb}^{3.5+}$. The valence of Tb ions in the $(\text{Pr}_{1-y}\text{Tb}_y)_{0.7}\text{Ca}_{0.3}\text{CoO}_3$ samples was simply deduced from observed intensity ratio I_D/I_C of the D to C spectral peaks,²² taking the data at 300 K as a standard of $\text{Tb}^{3.0+}$. This has been done with use of the calibration line in the inset of Fig. 3(b).

The fit of XANES spectra is exemplified in Fig. 4 using the data for the $(\text{Pr}_{0.8}\text{Tb}_{0.2})_{0.7}\text{Ca}_{0.3}\text{CoO}_3$ sample at 8 K, where the valence change achieves a maximum. It turns out that the XANES spectrum at Pr L_3 -edge is well reproduced within the energy range from 5944 to 5985 eV including the peaks related to Pr^{3+} and Pr^{4+} . The B2 component at the slope of main peak A is also resolved and the presence of $\text{Pr}^{3+}/\text{Pr}^{4+}$ mixture is thus obvious. Figure 4(b) shows the fit of the XANES spectrum at Tb L_3 -edge for the same sample, also at 8 K. The XANES spectrum cannot be reproduced without considering both characteristic peaks of Tb^{3+} and Tb^{4+} (features C and D, respectively).

The results based on the curve fitting of XANES spectra are summarized in Figures 5(a) and 5(b), which show, respectively, the temperature dependence of the valence of Pr and Tb ions in the $(\text{Pr}_{1-y}\text{Tb}_y)_{0.7}\text{Ca}_{0.3}\text{CoO}_3$ samples. Contrary to the sharp MI-SS transitions detected by the electric resistivity and magnetic susceptibility, the average Pr valence changes on cooling from 300 K gradually, though with the steepest increase at T_{MI} . Finally at the lowest temperatures, the valence reaches final values of 3.19+ and 3.25+ for the $y=0.1$ and 0.2 samples, respectively. The uncertainty of the estimated valence values is of about ± 0.03 , which arises from the arbitrariness of parameters used in the arctangent and Lorentzian functions. Comparing the results for $(\text{Pr}_{1-y}\text{Tb}_y)_{0.7}\text{Ca}_{0.3}\text{CoO}_3$ and those for the

$(\text{Pr}_{1-y}\text{Y}_y)_{0.7}\text{Ca}_{0.3}\text{CoO}_3$ samples ($y=0.075$ and 0.15)¹⁶ also presented in Fig. 5(a), one finds that the enhancement of the Pr valence systematically increases with increasing contents of the substitution with smaller Tb or Y ions, *i.e.* with decreasing of the mean size of the A-site cation in the perovskite structure.

As the Tb valence in $(\text{Pr}_{1-y}\text{Tb}_y)_{0.7}\text{Ca}_{0.3}\text{CoO}_3$ is concerned, it changes gradually around T_{MI} and reaches final values of 3.01+ and 3.03+ at 8 K for the $y=0.1$ and 0.2 samples, respectively (see Fig. 5(b)). We note, however, that the increase in the Tb valence is about one order of magnitude smaller and its gradual character is even more pronounced than in the case of Pr valence.

D. XANES measurements at RE edges for $(\text{Pr}_{1-y}\text{RE}_y)_{0.7}\text{Ca}_{0.3}\text{CoO}_3$ (RE=Sm, Eu)

To illustrate the valence states of the substituted Sm and Eu ions in $(\text{Pr}_{1-y}\text{RE}_y)_{0.7}\text{Ca}_{0.3}\text{CoO}_3$, the temperature dependent XANES spectra at the Sm L_3 -edge and Eu L_3 -edge are compiled in Figs. 6(a) and 6(b). The insets present the data on electrical resistivity $\rho(T)$ on the heating run, which demonstrate the existence of MI transition with characteristic temperatures T_{MI} of 86 K and 54 K for the RE=Sm and Eu samples, respectively. For the samarium substituted sample, although the intensity of the main peak of Sm^{3+} at 6720 eV slightly decreased with decreasing T , no isomeric shift or new spectral feature is detected. This result suggests that the Sm valence remains essentially as 3.0+ over the entire temperature range. For the europium substituted sample, the spectrum does not change at all down to 8 K and, consequently, the valence of the Eu ion also remains 3.0+.

E. Discussion

The unusual MI-SS transition occurring in some Pr-based cobaltites is intimately connected with a charge transfer between praseodymium and cobalt sites. Such process is enabled by energy closeness of the $\text{Pr}^{3+}/\text{Pr}^{4+}$ valence states. In the previous subsections, a possibility of more complex valence equilibria has been probed on $(\text{Pr}_{1-y}\text{RE}_y)_{0.7}\text{Ca}_{0.3}\text{CoO}_3$ systems with the RE=Tb, Sm, Eu substitutions at Pr-sites, in which mixed valence states, $\text{RE}^{3+}/\text{RE}^{4+}$ or $\text{RE}^{3+}/\text{RE}^{2+}$, can eventually also occur. Indeed, a small but unquestionable

increase in the valence of RE ion is observed for the Tb substituted samples below T_{MI} , besides the substantial enhancement of the Pr ion valence to 3.25+. On the other hand, no temperature variation of the Sm and Eu valence state is detected for such RE substituted samples.

To demonstrate the role of particular rare earths, the transition temperature T_{MI} has been plotted in Fig. 7(a) as a function of the average ionic radius of the perovskite A -site, $\langle r_A \rangle$. It is seen that the interrelation between T_{MI} and $\langle r_A \rangle$ is not universal, the curves gradually shift to the large $\langle r_A \rangle$ side with decreasing ionic radius of RE. In this comparison, the curve for RE=Tb is not peculiar, which can be understood, since the actual shift of Tb valence is fairly small (to 3.03+ in maximum). Nonetheless, the possibility of $\text{Tb}^{3+}/\text{Tb}^{4+}$ crossover in cobaltites is confirmed and additional studies aiming to exemplify this valence change are under study.

Finally, in Fig. 7(b) we plot the formal valence of Co ions at 8 K as a function of $\langle r_A \rangle$, calculated based on the Pr or Tb valences estimated from XANES data. It is seen that the doping level of the cobalt subsystem decreases from 0.30 hole per f. u. to about 0.15 hole per f. u., which is nearly independent on $\langle r_A \rangle$. The similar relation for other RE system was also shown, in which the valence of the Co ion is also independent on $\langle r_A \rangle$ and species of RE ion. As a final note we may mention that the T_{MI} vs $\langle r_A \rangle$ relation is applicable only for the $(\text{Pr}_{1-y}\text{RE}_y)_{0.7}\text{Ca}_{0.3}\text{CoO}_3$ systems and does not hold for the intensively studied system $\text{Pr}_{0.5}\text{Ca}_{0.5}\text{CoO}_{3-\delta}$, in which the Co, Pr valences and T_{MI} strongly depend on the actual oxygen content.^{4,15,17}

IV. CONCLUSION

Temperature dependence of the X-ray absorption near-edge structure (XANES) spectra at the Pr L_3 and RE L_3 edges was measured for the $(\text{Pr}_{1-y}\text{RE}_y)_{0.7}\text{Ca}_{0.3}\text{CoO}_3$ samples (RE=Tb, Sm and Eu), in which a metal-insulator (MI) and spin-state (SS) transition took place simultaneously at a critical temperature T_{MI} . The important experimental results and conclusions are summarized as follows.

(1) In all the studied Pr-based cobaltites, the trivalent praseodymium ions change to a $\text{Pr}^{3+}/\text{Pr}^{4+}$ mixture below T_{MI} , which anticipates that, at the same time, the formal cobalt valence should decrease from 3.3+ closer to 3.0+.

(2) Besides the enhancement of the Pr valence, a small increase in the valence of the Tb ion is found in the $(\text{Pr}_{1-y}\text{Tb}_y)_{0.7}\text{Ca}_{0.3}\text{CoO}_3$ samples below T_{MI} . In the $y=0.2$ sample, the average valence determined at 8 K makes 3.03+ and 3.25+ for the Tb and Pr ion, respectively. The calculated Co valence is 3.156+ in this case. It should be noted that these results do not necessarily mean very different tendencies of the two rare-earth ions for tetravalent states, since the final valence balance in such chemically inhomogeneous systems depends also on steric factors, including the size mismatch at perovskite A -sites.

(3) The observed valence shift of Tb ion indicates the energy closeness of trivalent and tetravalent states in this rare earth. This fact suggests that the unusual MI-SS transition need not be unique for the Pr-based cobaltites but can be expected also for the Tb-based ones.

(4) In the $(\text{Pr}_{1-y}\text{RE}_y)_{0.7}\text{Ca}_{0.3}\text{CoO}_3$ samples (RE=Sm and Eu) with similar MI-SS transition, no valence shift of the RE ion is detected at the RE ion absorption edge in the XANES spectra. This may signify that the energy closeness of trivalent and divalent states in these rare earths has no effect on the praseodymium/cobalt valence equilibria.

Acknowledgments

The synchrotron radiation experiments were performed at the BL01B1 of SPring-8 with approval of Japan Synchrotron Radiation Research Institute (JASRI) (Proposals Nos. 2011A1060, 2011B1075 and 2012A1118). Part of the work was performed under the financial support of a Grant-in-Aid for Scientific Research (No. 24540355) from the Ministry of Education, Culture, Sports, Science and Technology, Japan, and the Grant Agency of the Czech Republic within the Project No. 204/11/0713.

¹ Z. Jiráček, J. Hejtmánek, K. Knížek, and M. Veverka, Phys. Rev. B, 78, 014432 (2008).

² M. A. Korotin, S. Yu. Ezhov, I. V. Solovyev, V. I. Anisimov, D. I. Khomskii, and G. A. Sawatzky, Phys. Rev. B 54, 5309 (1996).

³ J. -Q. Yan, J.-S. Zhou, and J. B. Goodenough, Phys. Rev. B 69, 134409 (2004).

⁴ S. Tsubouchi, T. Kyômen, M. Itoh, P. Ganguly, M. Oguni, Y. Shimojo, Y. Morii, and Y. Ishii, Phys. Rev. B 66, 052418 (2002)

- ⁵ S. Tsubouchi, T. Kyômen, M. Itoh, and M. Oguni, Phys. Rev. B 69, 144406 (2004).
- ⁶ T. Saitoh, Y. Yamashita, N. Todoroki, T. Kyomen, M. Itoh, M. Higashiguchi, M. Nakatake, and K. Shimada: J. Electron Spectrosc. Relat. Phenom. 144?147, 893 (2005).
- ⁷ T. Fujita, T. Miyashita, Y. Yasui, Y. Kobayashi, M. Sato, E. Nishibori, M. Sakata, Y. Shimojo, N. Igawa, Y. Ishii, K. Kakurai, T. Adachi, Y. Ohishi, and M. Takata, J. Phys. Soc. Jpn. 73, 1987 (2004).
- ⁸ T. Fujita, S. Kawabata, M. Sato, N. Kurita, M. Hedô, and Y. Uwatoko, J. Phys. Soc. Jpn. 74, 2294 (2005).
- ⁹ T. Naito, H. Sasaki, and H. Fujishiro, J. Phys. Soc. Jpn. 79, 034710 (2010).
- ¹⁰ M. Maryško, Z. Jiráček, K. Knížek, P. Novák, J. Hejtmánek, T. Naito, H. Sasaki, and H. Fujishiro, J. Appl. Phys. 109, 07E127 (2011).
- ¹¹ T. Naito, unpublished.
- ¹² K. Knížek, J. Hejtmánek, P. Novák, and Z. Jiráček, Phys. Rev. B 81, 155113 (2010).
- ¹³ J. Wu and C. Leighton, Phys. Rev. B 67, 174408 (2003).
- ¹⁴ K. Knížek, Z. Jiráček, J. Hejtmánek, and P. Novák, J. Magn. Magn. Mater. 322, 1221 (2010).
- ¹⁵ J. Hejtmánek, E. Šantavá, K. Knížek, M. Maryško, Z. Jiráček, T. Naito, H. Sasaki, and H. Fujishiro, Phys. Rev. B 82, 165107 (2010).
- ¹⁶ H. Fujishiro, T. Naito, S. Ogawa, N. Yoshida, K. Nitta, J. Hejtmánek, K. Knížek, and Z. Jiráček, J. Phys. Soc. Jpn. 81, 064079 (2012).
- ¹⁷ J. L. García-Muñoz, C. Frontera, A. J. Barón-González, S. Valencia, J. Blasco, R. Feyerherm, E. Dudzik, R. Abrudan, and F. Radu, Phys. Rev. B 84, 045104 (2011); J. Herrero-Martín, J. L. García-Muñoz, S. Valencia, C. Frontera, J. Blasco, A. J. Barón-González, G. Subías, R. Abrudan, F. Radu, E. Dudzik and R. Feyerherm, Phys. Rev. B 84, 115131 (2011).
- ¹⁸ J. Herrero-Martín, J. L. García-Muñoz, K. Kvashnina, E. Gallo, G. Subías, J. A. Alonso, and A. J. Barón-González: Phys. Rev. B 86, 125106 (2012).
- ¹⁹ E. Largeau, M. El-Ghozzi and D. Avignant: J. Solid State Chem. 139, 248 (1998).
- ²⁰ M. Mizumaki, S. Tsutsui, H. Tanida, T. Uruga, D. Kikuchi, H. Sugawara and H. Sato: J. Phys. Soc. Jpn. 76, 053706 (2007).
- ²¹ C. Felser, J. Kohler, A. Simon, O. Jepson, G. Svensson, S. Cramm and W. Eberhardt: Phys. Rev. B 57, 1510 (1998).
- ²² H. Yamaoka, H. Oohashi, I. Jarrige, T. Terashima, Y. Zou, H. Mizota, S. Sakakura, T. Tochio,

- Y. Ito, E. Ya. Sherman, and A. Kotani, Phys. Rev. B 77, 045135 (2008).
- ²³ A. Bianconi, A. Marcelli, H. Dexpert, R. Karnatak, A. Kotani, T. Jo and J. Petiau, Phys. Rev. B 35, 806 (1987).
- ²⁴ Z. Hu, S. Bertram, and G. Kaindl, Phys. Rev. B 49, 39 (1994).
- ²⁵ B. Ravel, and M. Newville, J. Synchrotron Rad. 12, 537 (2005).
- ²⁶ H. Dexpert, R.C. Karnatak, J.M. Esteve, J.P. Connerade, M. Gasgnier, P.E. Caro and L. Albert: Phys. Rev. B 36, 1750 (1987).
- ²⁷ J. B. Gruber, K. L. Nash, R. M. Yow, D. K. Sardar, U. V. Valiev, A. A. Uzokov, and G. W.Burdick: J. Lumines. 128, 1271 (2008).
- ²⁸ G. Kalkowski, G. Kaindl, G. Wortmann, D. Lentz and S. Krause: Phys. Rev. B 37, 1376 (1988).

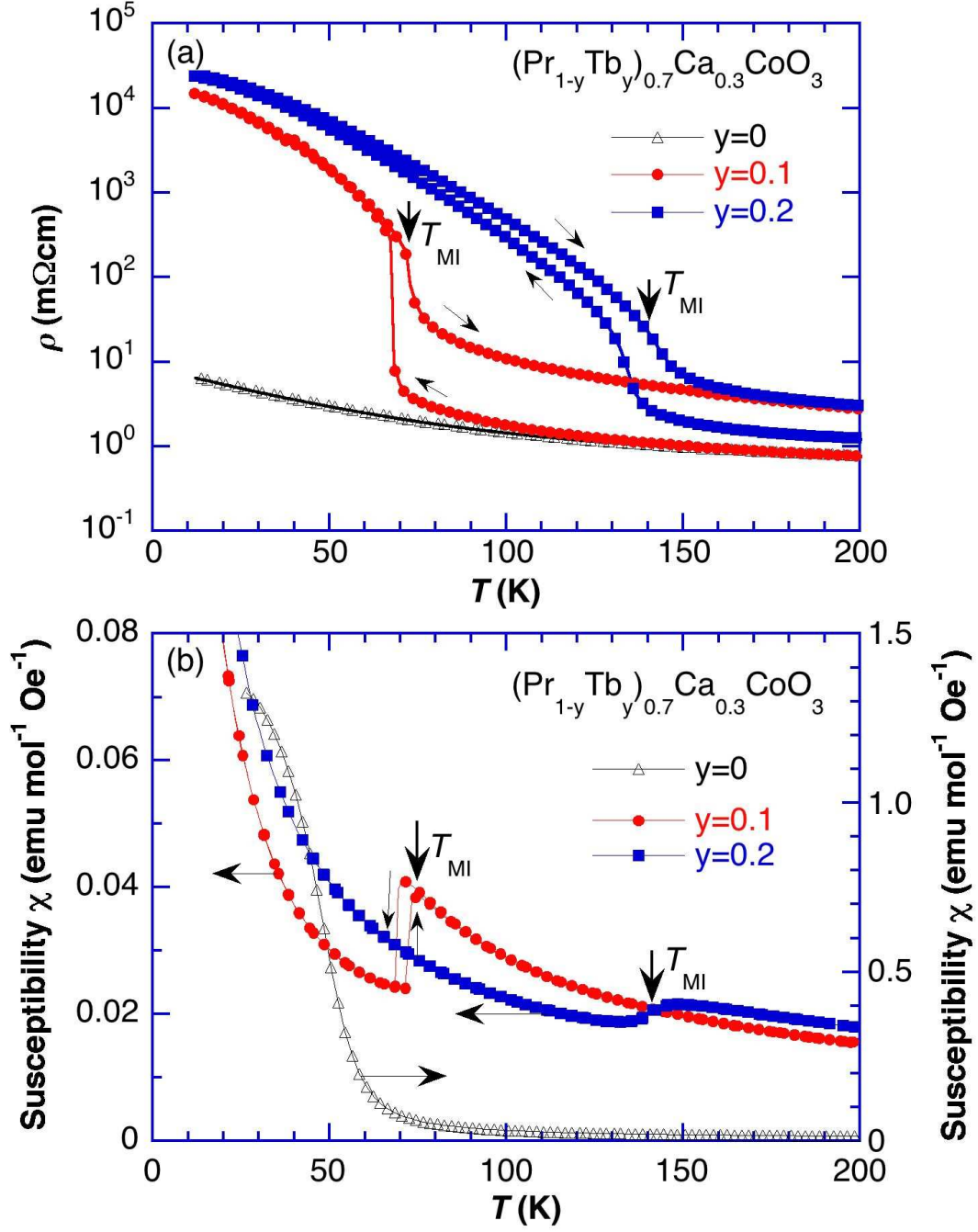


FIG. 1: Temperature dependence of the (a) electrical resistivity $\rho(T)$ and (b) magnetic susceptibility $\chi(T)$ for the $(\text{Pr}_{1-y}\text{Tb}_y)_{0.7}\text{Ca}_{0.3}\text{CoO}_3$ samples ($y=0, 0.1$ and 0.2).

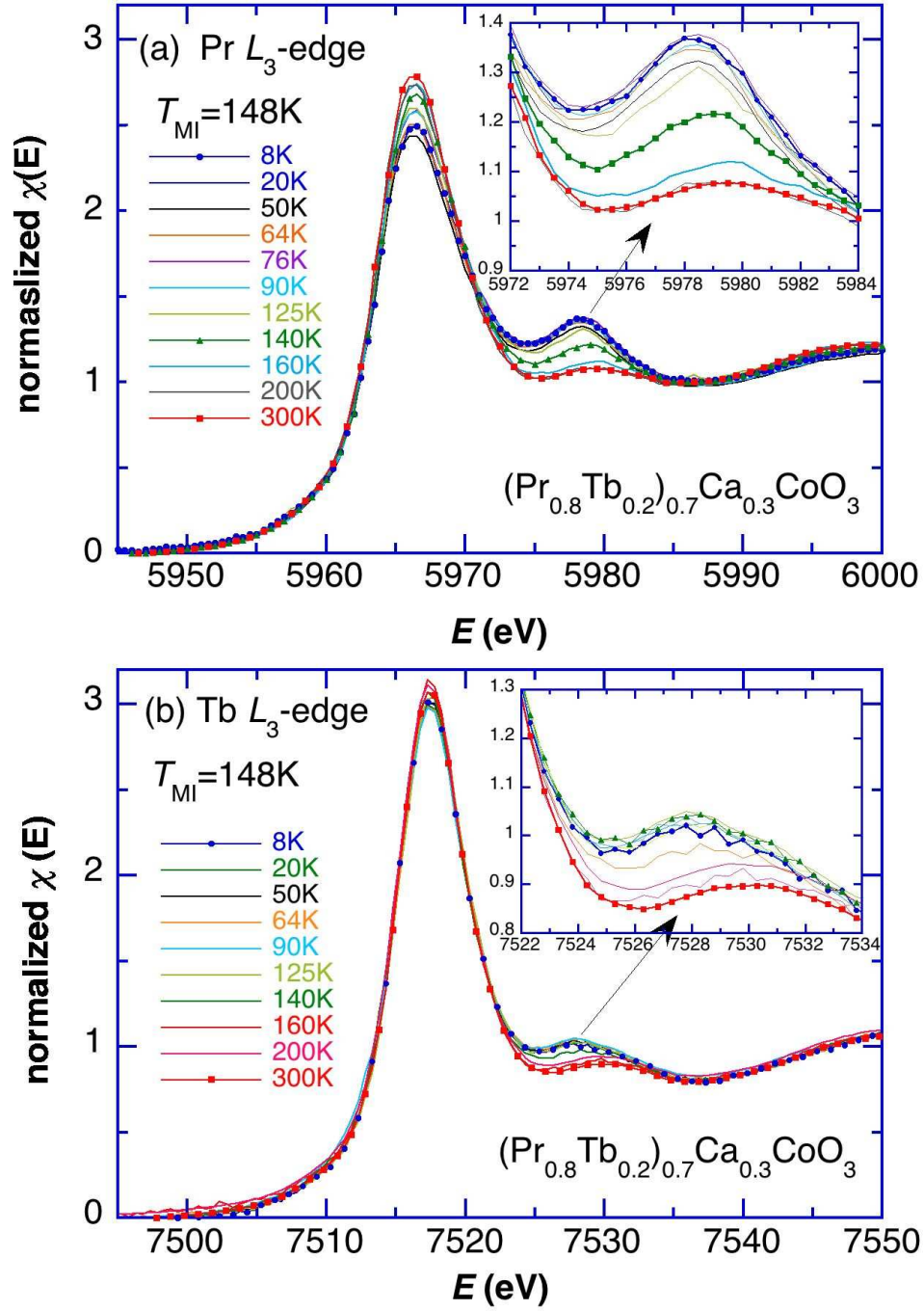


FIG. 2: Temperature dependence of the XANES spectra at the (a) Pr L_3 -edge and (b) Tb L_3 -edge for the $(\text{Pr}_{0.8}\text{Tb}_{0.2})_{0.7}\text{Ca}_{0.3}\text{CoO}_3$ sample. Insets show the magnification around the $4f^1$ and $4f^7$ spectra related with the Pr^{4+} and Tb^{4+} ions, respectively.

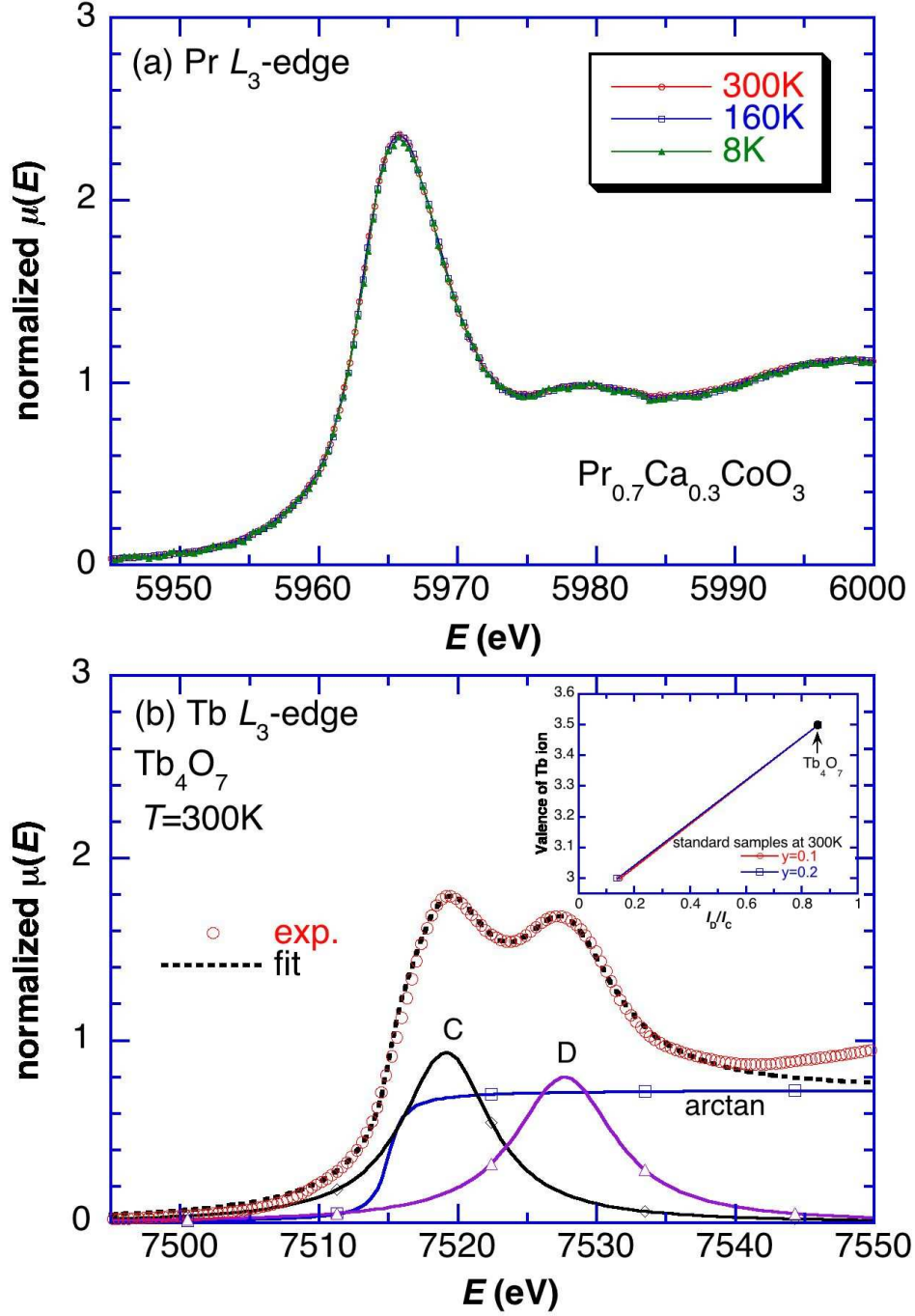


FIG. 3: (a) Temperature dependence of the XANES spectra at the Pr L_3 -edge for $\text{Pr}_{0.7}\text{Ca}_{0.3}\text{CoO}_3$. (b) The XANES spectrum for Tb_4O_7 at 300 K, fitted by a sum of two Lorentzian functions (peak C for Tb^{3+} and peak D for Tb^{4+}) and one arctangent function.

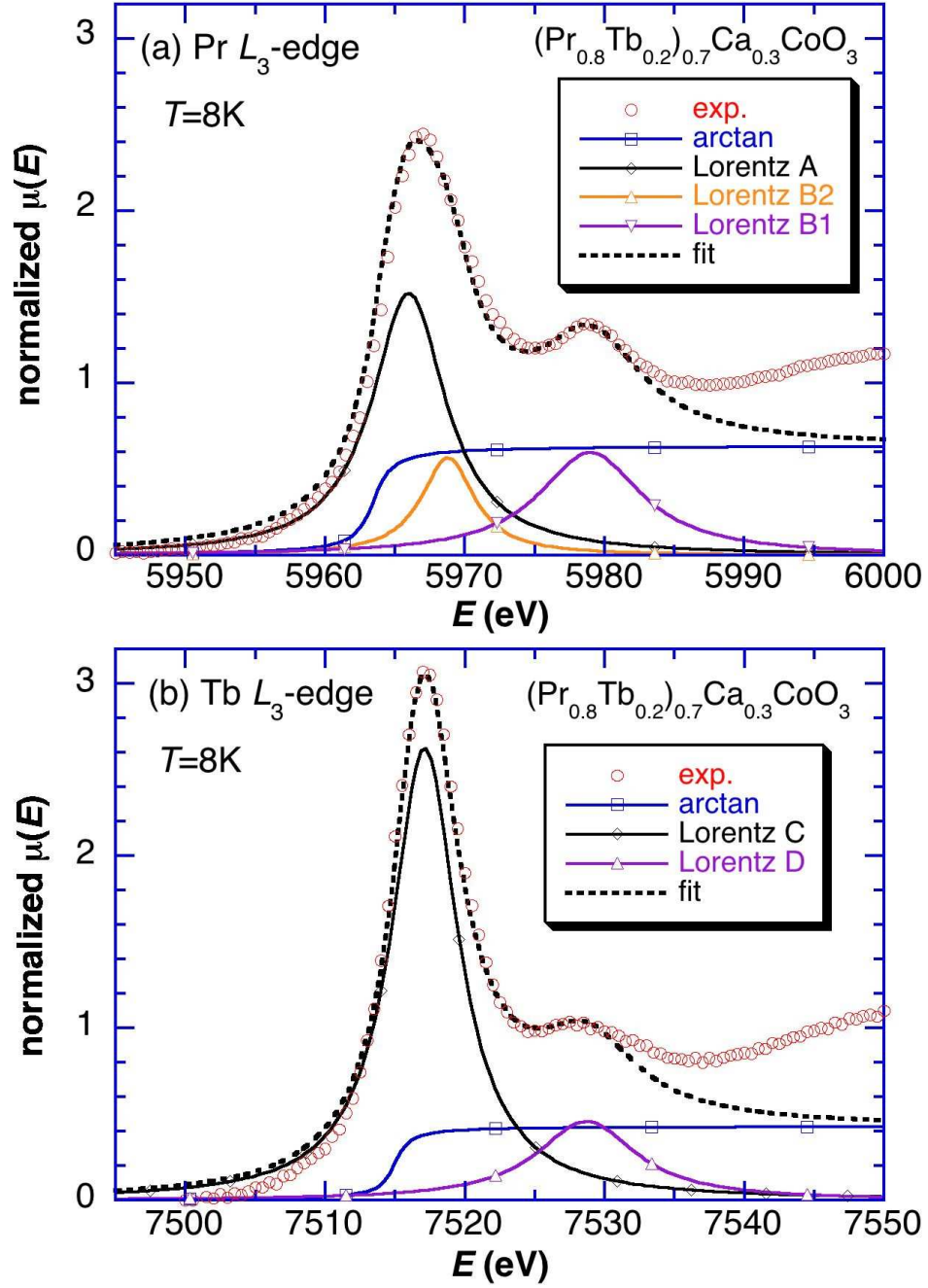


FIG. 4: Examples of the fitting of the XANES spectrum at the (a) Pr L_3 - and (b) Tb L_3 -edge for the $(\text{Pr}_{0.8}\text{Tb}_{0.2})_{0.7}\text{Ca}_{0.3}\text{CoO}_3$ sample at 8 K. For the fitting of the Pr L_3 -edge, one arctangent function and three Lorentzian functions (A, B1 and B2) are used. For the fitting of the Tb L_3 -edge, one arctangent function and two Lorentzian functions (C and D) are used.

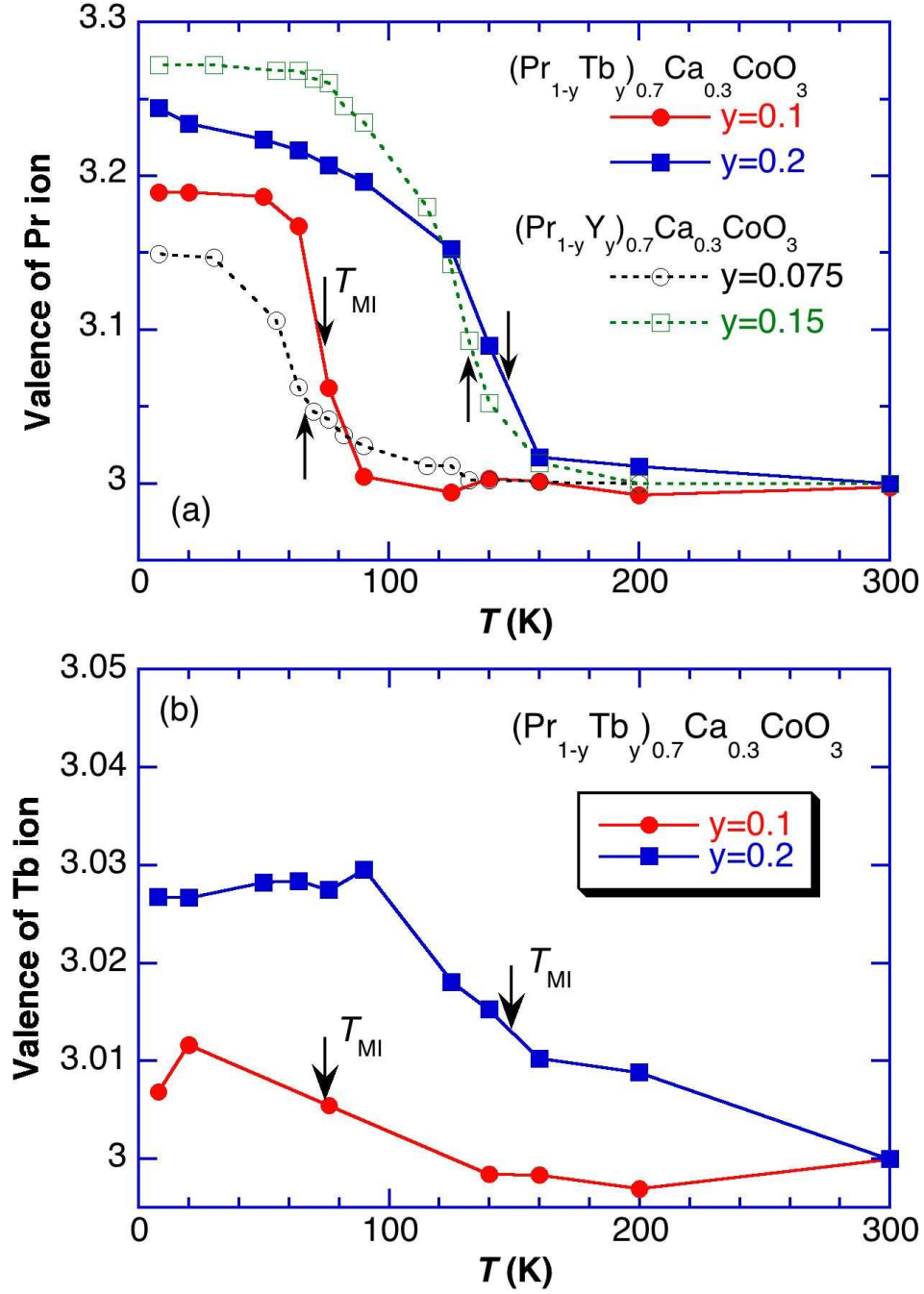


FIG. 5: Temperature dependence of the average valence of (a) Pr ion and (b) Tb ion for the $(\text{Pr}_{1-y}\text{Tb}_y)_{0.7}\text{Ca}_{0.3}\text{CoO}_3$ samples estimated using the XANES spectra and curve fitting. In (a), the estimated valence of Pr ion for the reported $(\text{Pr}_{1-y}\text{Y}_y)_{0.7}\text{Ca}_{0.3}\text{CoO}_3$ samples ($y=0.075$ and 0.15)¹⁶ is also presented.

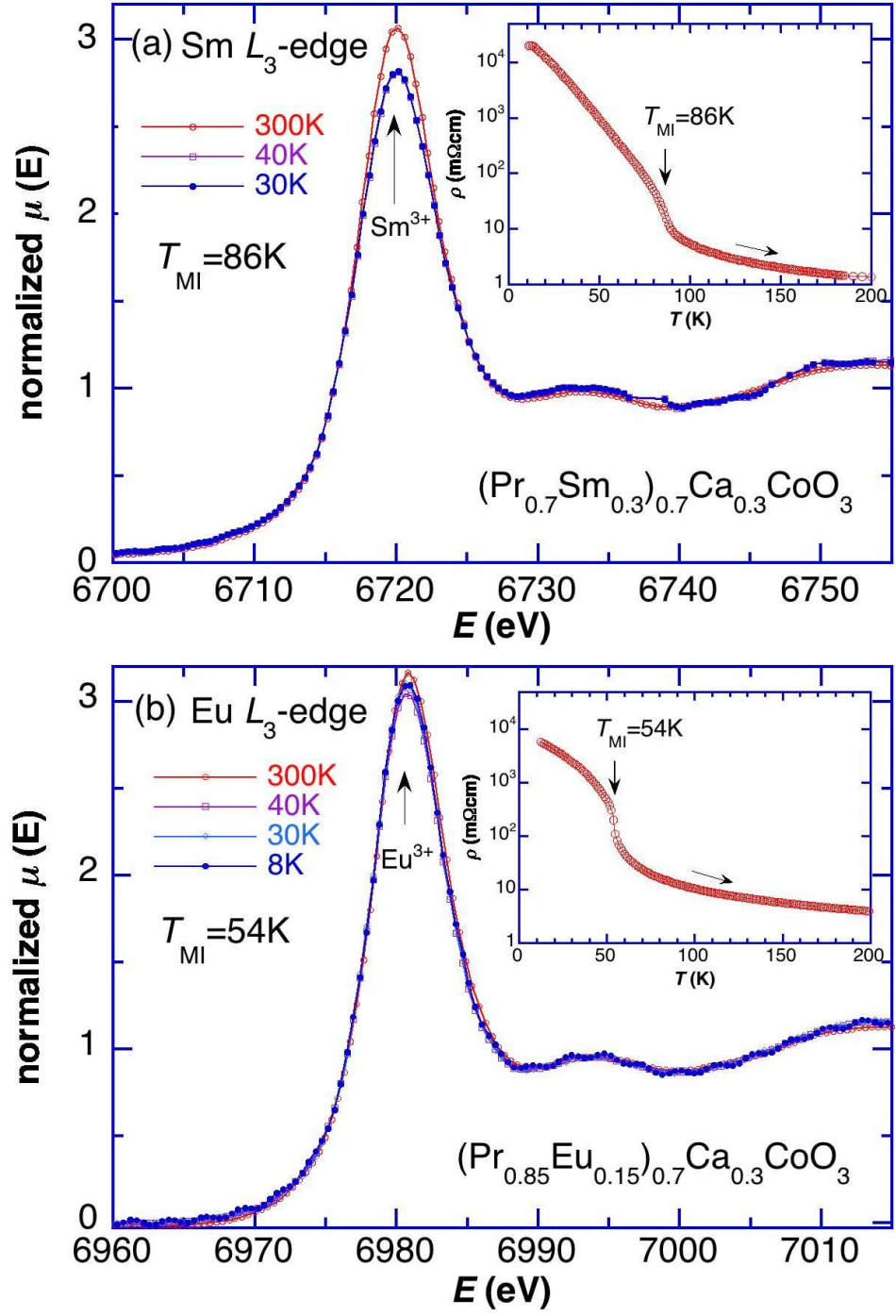


FIG. 6: Temperature dependence of the XANES spectra at (a) Sm L_3 -edge for $(\text{Pr}_{0.7}\text{Sm}_{0.3})_{0.7}\text{Ca}_{0.3}\text{CoO}_3$ and (b) Eu L_3 -edge for $(\text{Pr}_{0.85}\text{Eu}_{0.15})_{0.7}\text{Ca}_{0.3}\text{CoO}_3$ samples.

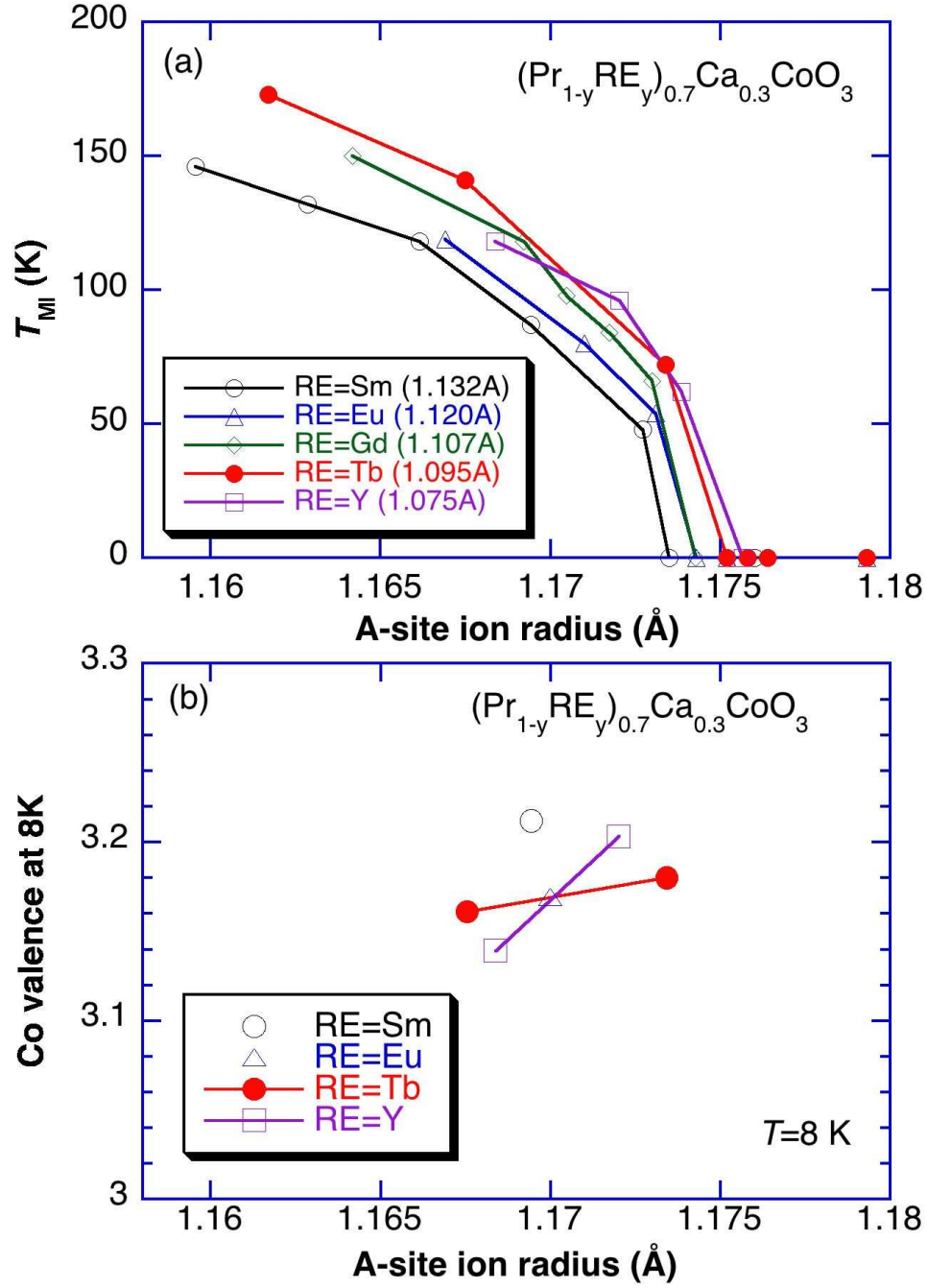


FIG. 7: (a) The transition temperature T_{MI} and (b) the calculated valence of Co ion at 8 K, as a function of the average ionic radius of the perovskite A -site, $\langle r_A \rangle$ for various $(\text{Pr}_{1-y}\text{RE}_y)_{0.7}\text{Ca}_{0.3}\text{CoO}_3$ systems.